5-2018

Enhancing performance of ionic liquid property prediction with molecular dynamics.

Trisha H. Patel
University of Louisville

ENHANCING PERFORMANCE OF IONIC LIQUID PROPERTY PREDICTION WITH MOLECULAR DYNAMICS

By

Trisha H. Patel
B.S., University of Louisville, 2014

A Thesis
Submitted to the Faculty of the
University of Louisville
J.B. Speed School of Engineering
as Partial Fulfillment of the Requirements
for the Professional Degree

MASTER OF ENGINEERING

Department of Chemical Engineering

May 2018

ENHANCING PERFORMANCE OF IONIC LIQUID PROPERTY PREDICTION WITH MOLECULAR DYNAMICS

Submitted by:

_____

Trisha H. Patel

A Thesis Approved On

_____

May 20, 2018

by Following Reading and Examination Committee:

_____

Vance W. Jaeger, Thesis Director

_____

James C. Watters

_____

Angela K. Thompson

ACKNOWLEDGMENTS

Parents are the leading force to why most strive for success, I am thankful for getting the opportunity to be encouraged and pushed to my upmost success. I would like to thank all instructors through my career that have given me the opportunity to take on challenges. This allowed me to blossom into the world with respect and integrity.

ABSTRACT

Molecular dynamics have been used to predict thermodynamic and transport properties of eight room-temperature ionic liquids. Simulation parameters including box size and van der Waals cutoffs were varied. The density, heat capacity, and self-diffusion coefficients of the ionic liquids were computed and compared to experimental data and to previously published simulations. Predicted properties were generally close to their experimentally observed values. It was determined that the prediction of ionic liquid properties via molecular dynamics simulations could be accelerated several-fold by using less stringent integration parameters and smaller simulation sizes. The properties of density and heat capacity did not change significantly even with the least computationally expensive parameters tested, whereas diffusion coefficients were impacted by smaller box sizes. These results indicate that several important properties of ionic liquids can be predicted much more quickly than previously thought, thus improving large-scale computational screening of ionic liquids and other novel solvents.

TABLE OF CONTENTS

LIST OF TABLES

TABLE **PAGE**

LIST OF FIGURES

FIGURES **PAGE**

I. INTRODUCTION AND BACKGROUND

Ionic liquid (ILs) solvents consisting of organic salts in which the ions within are poorly coordinated result in a low melting point. Therefore, ILs are defined to be any salt that is a liquid below 100^{o}C. Alternatively, a smaller class of ILs remain liquid at room temperature (room temperature ionic liquids, RTIL's). At minimum one ion within the salt has a delocalized charge, usually an organic moiety, preventing stable crystal lattice

formation[1]. ILs contain free ions which make them electrically conducting, meaning they dissolve specific substances with readily available solvents, and they tend to be chemically stable with a low vapor pressure resulting in an increased delocalized efficiency rate [2]. Each of these properties make ILs attractive for various industrially relevant processes.

The first synthesized Protic ionic liquid (PIL), as shown in figure 1, was ethanol ammonium nitrate with a melting point of around 50^{o}C, created by S. Gabriel and J.Weiner in the 1880s[3]. Thirty years later Paul Walden, also well known for Walden inversion within organic chemistry[4], substituted the hydroxyl group with a methyl group, within ethanol ammonium nitrate, resulting in a decreasing overall attraction leading to lowering the melting point[4]. In the 1970s and 1980s, pyridinium cations with halogen anions were synthesized and used as electrolytes in batteries; however they were found to decompose in an aqueous acidic or alkaline environment. Thus, these ILs were not suitable for long-term use. In the 1990s more stable ionic liquids were synthesized by Wilkes and Zawarotko including the phosphorus hexafluoride anion and the boron tetrafluoride anion[5]. While these ions were highly stable, they were found to be toxic.

Ionic liquids can be used as solvents in non-aqueous reactions. For example, in the Friedel-Crafts reaction they are used as a catalyst to synthesize branched alkanes by dimerization of shorter alkenes[6]. The first large scale application was in the BASIL process developed by BASF in which the ionic liquid was used to remove acidic residue allowing acid free recovery of the product[7]. Ionic liquids can be used in dissolving cellulose and lipids with a goal of producing biofuels. There has also been considerable interest in the use of ILs for the capture and processing of carbon dioxide.

There are thousands of possible binary IL combinations and millions of tertiary or quaternary combinations. The properties of ILs tend not to follow easy mixing rules, thus they are difficult to accurately predict with simple quantitative structure activity relationships (QSAR) methods. Such a large library of solvents cannot be synthesized and tested in a lab setting without great cost in time, effort, and money. An alternative to laboratory testing is computational screening, which can be scaled very easily to hundreds or thousands of computers. Macroscopic properties of a single IL solvent can be predicted from its molecular descriptions in a matter of several hours on a single desktop computer. By comparison, it could take a synthetic chemist days to synthesize and test a single IL.

Molecular dynamics (MD) is a method used to simulate the dynamics of molecular systems over time through the integration of Newton's equations of motion. Over the last several decades, MD has progressed from a method used to demonstrate statistical mechanical theory to a widely applied chemical research tool[8]. Computer simulations bridge microscopic length and time scales with macroscopic laboratory experiments. Properties of solvents (e.g. density, heat capacity, and viscosity) predicted with MD can be tested against experimental values that appear in publications or literature. Accurate MD simulations require a good description of molecular interactions, which are compiled for groups of related molecules in a set known as a force field. For ILs, the General Amber Force Field (GAFF) has been shown to accurately reproduce the properties of many ILs — within a few percent of error for some properties. Recently, MD simulations have been used more frequently to eliminate difficult or nearly impossible laboratory experiments. For example, extreme temperatures and pressures are not suitable for most laboratory

experiments due to insufficient safety protocols; however, the simulations do not experience the same degree of limitation through the computationally-generated process.

Molecular dynamics can be implemented in a multitude of software packages. The GROningen Machine for Chemical simulations (GROMACS) is one of the most commonly used MD engines in academia, because it is among the fastest and most reliable packages, typically running 3-10 times faster than many competitors. GROMACS is free to download, use, edit, and distribute, making it attractive for academic researchers. GROMACS allows the simulation of Newtonian equations of motion for systems with hundreds to millions of dynamic particles with many modern algorithms and techniques supported. The package was designed to probe biochemical molecules including proteins, lipids, and nucleic acids. Through practice and implementation, GROMACS has been found to be extremely proficient in the calculation of nonbonded interactions (electrostatics and van der Waals), rapidly leading to its adoption for applications in non-biological systems (e.g. ionic liquids).

GROMACS is accessed through a command-line interface, within the software, used for file input and output. Providing calculation progress and estimated time of completion feedback is one of the key reasons GROMACS is being used for the present IL study. In addition to the MD engine that integrates equations of motion, GROMACS also contains an extensive library for trajectory analysis, which allows for fast and accurate calculation of solvent properties. GROMACS has hundreds of consistency checks programmed into its packages, disallowing settings that would produce inaccurate or unviable data. After creating the input files (IL solvents) the simulation runs over several hours to produce a trajectory file. The trajectory file contains snapshots of the molecular

coordinates of the system, thus detailing the movements of the atoms over time. In addition to the molecular positions, the simulation reports statistics about properties such as pressure, temperature, enthalpy, and density, which are important for later analysis. Output data files can be examined through GROMACS' built-in packages or through visualization with a program such as VMD.

A variety of cation and anion force fields have been designed to model properties of specific ILs. To increase efficiency in prediction of thermophysical properties of different ILs, molecular simulations--in particular MD simulations--can be utilized. The reliability of these predictions is dependent on the validity of the force field used to describe the intra- and intermolecular (bonded and non-bonded) interactions of the solvent molecules [6]. Bonded and non-bonded potentials will be described in detail later in this section. To reproduce experimental data for both biological and synthetic organic molecules, certain force fields have been optimized based on investigations from research and publications. Among these force fields are OPLS, CHARMM, UFF, AMBER and its companion the general AMBER force field[2] (GAFF). ILs usually consist of chemical elements and bond types similar to those used to parameterize these force fields. The work presented here uses GAFF in whole for bonded and van der Waals potentials with electrostatic potentials derived from in-house calculations. A comprehensive evaluation of GAFF was previously performed to determine how well this standard force fields behaves for a new class of solvents with no parameter optimization beyond that of the electrostatic parameterization. This previous study indicated that GAFF is an appropriate model for ILs. The current study is aimed at increasing the efficiency of similar calculations without affecting the accuracy of IL property prediction. Increases in efficiency were achieved

through using less stringent integration parameters and by reducing the size of the simulated system, as presented in full detail herein.

II. METHODS AND THEORY

Under ideal conditions (298.15 K and 1 bar), molecular dynamics simulations were conducted applying a combination of eight unique of ionic liquids including, anions of acetate [Ac], formate [HCO_2], and bis[(trifluoromethyl)sulfonyl] imide [Tf_2N] along with cations of alkylammonium [RAM], 1-alkyl-3-methylimidazolium [RMIM] and pyridinium [Pyr]. Calculations of IL density, heat capacity, and self-diffusivity have been

computed for the ILs and compared to experimental data and previously published simulations. The IL cations and anions are represented within Figure 1.

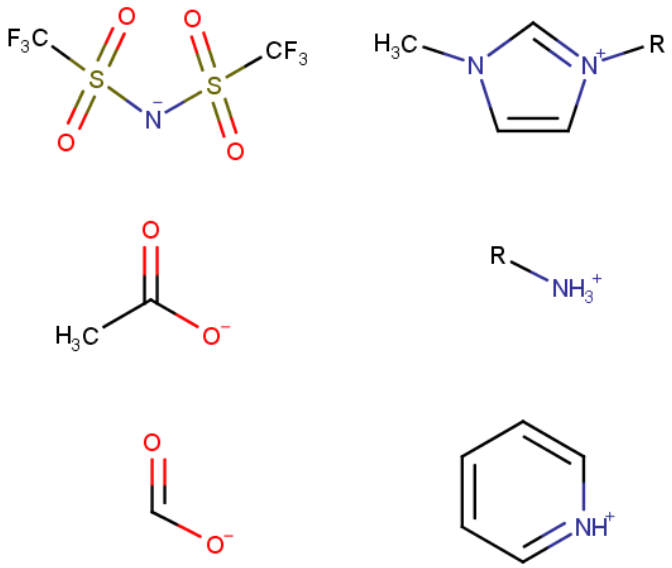

Figure 1: Ions used in this study.

R= ethyl (Et or E), butyl (B), pentyl (P), hexyl (H), and octyl (O).

I. Force Field Functional Form

The potential energy of the molecules in the system can be described by a force field which inputs the intramolecular bond lengths, bond angles, torsional angles, and intermolecular distances for non-bonded van der Waals and electrostatic interactions. The force field is a collection of equations and associated constants designed to reproduce molecular geometry and selected properties of tested structures[9-10]. The molecular interactions can be broken up into two sets, bonded and nonbonded. Bonded parameters

consist of bonds, angles, and dihedrals[2]. Bond angles and improper terms have similar quadratic forms, but with softer spring constants, allowing for easier stretching process . The force constants can be obtained from vibrational analysis of the molecule (experimentally or theoretically)[9-10]. The Lennard-Jones form is used to calculate the 12-6 (i.e. van der Waals) interactions and a columbic point-charge potential is used for electrostatic interactions[11]. Combining the bonded and non-bonded energies results in the overall potential energy of the system. For the ILs tested here, all necessary parameters for calculation of the bonded and Lennard- Jones terms are within GAFF, leaving electrostatic point charges to be identified. Strong electrostatic interactions, due to the presence of ionic species, lead to many of the important thermophysical properties of ILs. Therefore, to calculate IL properties accurately, electrostatic interactions must be accurately represented by the force field models.

GAFF is the force field utilized within the simulations for the 8 ILs studied here. The force field is detailed in equation 1. GAFF is based on AMBER, which is a set of molecular mechanical force fields used for simulations of biomolecules such as proteins and nucleic acids. Though very popular, AMBER initially lacked the parameters necessary to preform studies on many organic molecules. GAFF was developed to improve AMBER by expanding its applicability. GAFF was designed to describe organic molecules such as those within ILs, along with others such as drug molecules and protein ligands.

$$v_{t^0t} = \sum_{bonds} k_r\left(r - r_{eq}\right)^2 + \sum_{angles} k_\theta\left(\theta - \theta_{eq}\right)^2 +$$

$$\sum_{dihedrals} \frac{v_u}{2}\left[1 + \cos(n\phi - \lambda)\right] + \sum_{i<j}\left[\frac{A_{ij}}{R_i j^{12}} - \frac{B_{ij}}{R_i j^6} + \frac{q_i q_j}{\varepsilon R_{ij}}\right] [1]$$

Bond stretching and angle bending within GAFF are evaluated using a simple harmonic functional form while the dihedral term is evaluated using a cosine function in agreement with the AMBER functional form. For atoms in separate molecules or for atoms in the same molecule separated by a minimum of three bonds, electrostatic and van der Waals nonbonded interactions are calculated using Coulombic and 12-6 Lennard-Jones terms, considering all pairs of atoms (*i* and *j*) in the system. A scalar factor of 5/6 is used to reduce non-bonded interactions of atoms separated by exactly three bonds. Parameters included in the force field are (a) spring-like constants such as k_r, $k\theta$, and V_n, (b) the equilibrium structural parameters such as r_{eq} and θ_{eq}, (c) the particle atomic charges q_i and q_j derived from electronic structure calculations, (d) the Lennard-Jones well depth, ε, and radii, A_{ij} and B_{ij}, and (e) and torsional parameters for phase and multiplicity, n and λ.

II. Difficulties with Electronic Structure

The molecular transport properties of ILs are not described well with force fields when full $+e/-e$ charges are given to the cations and anions[12]. To determine the electronic point charge calculations are derived from quantum calculations within a vacuum as described below. The description of a cation or anion within a vacuum with a full charge does not accurately represent the electrostatic landscape of the liquid system. Within a liquid, the charge density of a molecule can be drastically affected by nearby molecules of the opposite charge due to molecular polarizability causing nearby molecules to screen charge. As a result, it was suggested that classical force fields should assume that there is a fraction of $+e/-e$ charges of the cation and anion[13]. Scaling of the ionic charge to some fraction of $+e/-e$ is required to accurately calculate shear viscosity or self-diffusivity of an IL using the

MD. Crystal structures of solidified ILs can be used in *ab initio* MD to calculate the electronic structure at great cost. These more expensive calculations tend to be more accurate for liquid structures, because the liquid is more comparable to the solid than to the gas (*in vacuo*). Previous *ab initio* studies of solid crystals indicate that multiplying the charges by a factor of 0.7-0.9[14] can create force fields with appropriate electrostatic interactions that reproduce dynamic properties of ILs well. By using MD rather than *ab initio* methods, IL properties can be predicted on a large-scale through molecular simulation. However, some accuracy is sacrificed through a coarser description of interactions. For the simulations presented herein, a scaling factor of 0.8 was used in accordance with previous studies that tested GAFF with ILs.

III. Quantum Mechanical Calculations

The electronic structure of each ion was calculated with quantum mechanical methods. An electronic structure program, Gaussian, was used to perform geometry optimization and energy calculations through Hartee-Fock (HF) level of theory implementing 6-31G(d)//6-31G(d) basis set. The GAFF force field was utilized to determine all force constants and equilibrium, along with Lennard-Jones parameters[2]. Electrostatic point charges were assigned using antechamber[15] by the RESP method and input files were created for each ion following. A scaling factor of 0.8 was multiplied by the atomic charges. The scaling method is universal in implication as Maginn and co-workers[16] along with Sprenger and Jaeger[2] utilized this within MD simulations.

IV. Preparation of MD Simulations

To build structures and force fields in a GROMACS-compatible format, an in-house script that combines the functionality of several other programs was used. First, GaussView, which contains a graphical user interface, was used to draw molecular structures. These structures were piped to a program called Gaussian which calculates the electronic structure of the individual molecules at the HF/6-31G(d) level of theory in a vacuum. This level of theory has been shown to accurately represent polarization of organic molecules, and it is the preferred level of theory for AMBER parameterization. The output of Gaussian can be interpreted by a program called antechamber which projects the electronic structure onto the atoms as point charges with the RESP method. Additionally, antechamber analyzes the molecular structure and assigns force field parameters from GAFF. Finally, a program called Acpype is used to generate MD input files in a GROMACS-compatible format, and charges were scaled by a factor of 0.8. Simulation boxes containing hundreds of pairs of anions and cations were packed using the Packmol program. Table 1 details the order of steps taken to prepare and run the simulations. A full 5 nm box of water and the ionic liquids are demonstrated in figure 2.

Table 1: Procedure for performing and analyzing a molecular simulation of an IL using GROMACS in this study.

Prepare the system	Create molecular structure (GaussView) Calculate electronic structure (Gaussian) Calculate point charges (Antechamber) Generate force fields (Acpype) Scale charges (awk) Pack a box of molecules (Packmol)
Simulation	Energy minimization (GROMACS - mdrun) High temperature MD (GROMACS - mdrun) Production STP MD (GROMACS - mdrun)
Outputs	Molecular trajectory (.trr and.xtc files) Energy (energy.xvg) Log file (md.log)
Analysis	Density (GROMACS – energy) Heat capacity (GROMACS – energy) Diffusion coefficient (GROMACS – msd) Speed of calculation (md.log file)

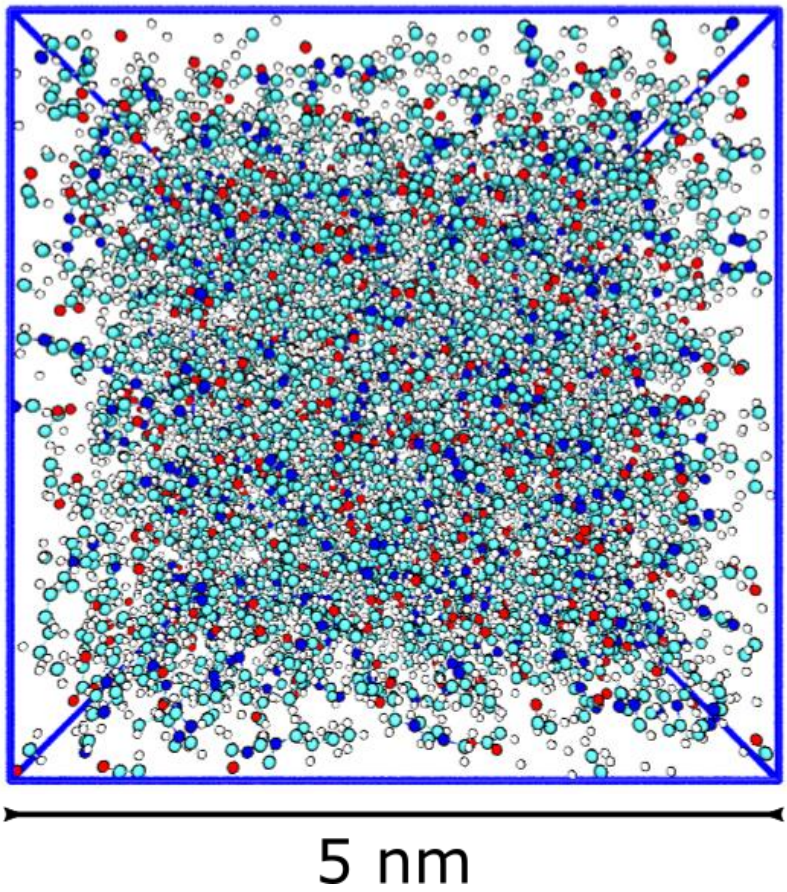

Figure 2: GROMACS MD run of an ion in a 5 nm box of water.

IL force fields can thus be constructed rapidly and with ease. With this method, screening for the optimal ILs for certain applications can be accomplished with greater efficiency. These simulations can also lead to the discovery of new ILs by testing hypothetical IL combinations that are difficult to synthesize in the lab. Moreover, properly parameterized simulations can explore complex interactions between solutes and ILs. Despite a potential, modest loss of accuracy, the MD approach is the optimal choice moving forward due to its low difficulty of implementation using widely available and free programs.

V. MD Simulations

Starting structures were constructed in cubic boxes containing 200-1000 ion pairs. The size of the box was varied across the simulations. Side lengths on the cubic boxes were varied in this study. Side lengths of 3, 5, and 10 nm was used. Using GROMACS 5.0.3 IL boxes were simulated with periodic boundary conditions. Long-range electrostatic interactions were calculated through the implication of particle-mesh Ewald (PME) summation. Short-range electrostatics were calculated explicitly. Van der Waals interactions were shifted to zero at a given cutoff distance. This distance was varied across the simulations. Cutoff lengths of 0.8, 1.0, 1.2, and 1.4 were used. The distances bonds between hydrogen and heavy atoms were constrained at their equilibrium values.

Energy minimization was carried out for 1000 steps using the steepest descent method. Each of the eight ILs was simulated in the NVT ensemble (nonstant number of atoms, volume, and temperature) for 10ns at 500K to achieve thorough mixing of the ions. This eliminated any artifacts in the initial configurations, creating coordinates independent of the Packmol input. Following the NVT simulations, snapshots were taken at 6, 8, and 10 ns to become inputs for further production simulations. Structures then underwent 10 ns of production simulation in the NPT (constant number of molecules, pressure, and temperature) ensemble. The first 6 ns of these simulations was ignored to allow for pressure equilibration before analysis was undertaken. NPT simulation were at room conditions (298.15 K and 1 bar), using the Berendsen barostat[2].

After the simulations completed, the GROMACS energy file was analyzed for box sizes (3, 5, and 10 nm) and cutoffs of (0.8, 1.0, 1.2, and 1.4 nm). Density, enthalpy fluctuations, and the number of molecules have recorded. A total of 21 simulations were completed for

this study. The reported density and heat capacity values represent the values averaged across three different simulations replicas.

Density

The density of each IL was computed using the mass of the box divided by the equilibrium volume of the simulation cell and are presented in Table 2 and 3, graphically shown in figure 3. Multiple simulations were run, to increase confidence in the results, from which an average of the data points was taken.

Heat Capacity

Constant pressure heat capacities for the ILs, were calculated using the classical definition represented in the equation below, using the RMSD of enthalpy as the numerator.

$$C_p = \left(\frac{\langle(\partial H)^2\rangle}{nk_\beta T^2}\right)_P = \left(\frac{<H^2>-<H>^2}{nk_\beta T^2}\right)_P \qquad [2]$$

H is enthalpy, temperature is *T*, k_B is Boltzmann's constant, and *n* is the total number of molecules. All values were extracted from GROMACS simulations. An average was taken across the replicas for each IL. Calculated values and corresponding experimental values for five of the eight ILs are reported in Tables 4 and 5 and graphically represented in Figure 4. Standard deviation of the three values is presented as the error.

Self-Diffusivity

Force fields lag in determining transport properties with accuracy, unlike predicting thermodynamic properties, where simulations mimic experiments quite well. Thus, in evaluating the accuracy of a force field, it is essential to calculate some dynamic property,

such as self-diffusivity to complement calculations of static and equilibrium properties. The self-diffusivity of the cations and anions is calculated via the mean square displacement, or MSD, of the ion centers. The Einstein relation, shown in the equation below, describes diffusivity, D, as a function of MSD. The angle-bracketed term is the MSD with respect to the molecular coordinates (r) over time (t), and the factor of 1/6 arises for a three-dimensional system.

$$D = \frac{1}{6}\lim_{t\to\infty}\frac{d}{dt} < \sum_{i=1}^{N}[r(t) - r(o)]^2 > \qquad [4]$$

III. RESULTS AND DISSCUSION

Density: A comparison of results for IL density and heat capacity of boHt box size and cutoff parameters is shown through parity plots in Figure 3. Error with respect to experimental values tends to be low, with most simulated densities falling within a few percent of their experimental values no matter which tested parameters are used.

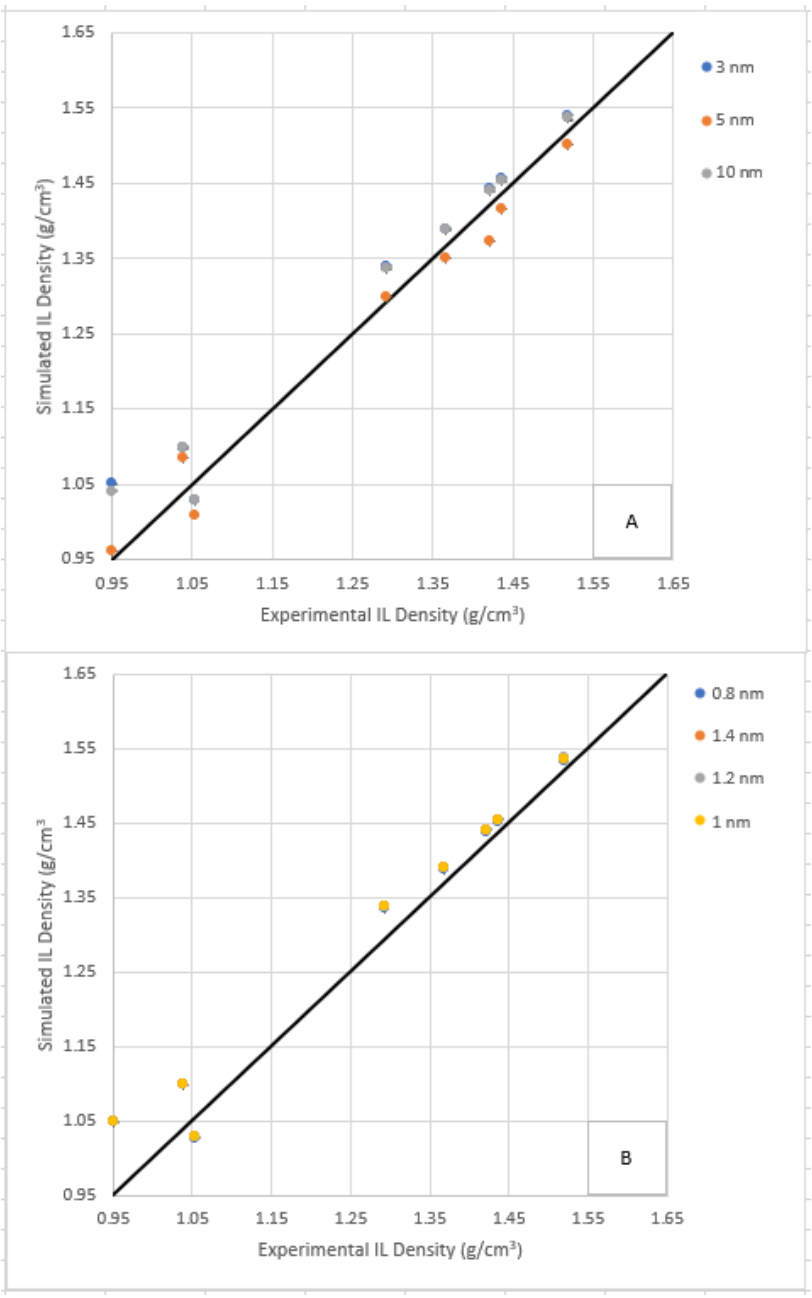

Figure 3: Experimental vs. simulated IL properties: (A) density with box size (g/cm ^{3}); (B) density with cutoff.

Table 2: Simulation IL density (g/cm^3) compared to experimental values from literature. An average density is determined for each box size parameter. Percent error determined through individual comparison[17-29].

Box Size (nm)		**3**		**5**		**10**	
IL	*Exp*	*Sim*	*E (%)*	*Sim*	*E (%)*	*Sim*	*E (%)*
[BMI][Ac]	1.053	1.030	2.158	1.010	4.084	1.029	2.240
[EAM][HCO_2]	1.039	1.100	5.852	1.085	4.427	1.099	5.758
[PAM][HCO_2]	0.950	1.051	10.651	0.962	1.263	1.041	9.588
[BMI][Tf_2N]	1.436	1.457	1.461	1.416	1.393	1.453	1.209
[EMI][Tf_2N]	1.519	1.539	1.311	1.501	1.185	1.537	1.170
[HMI][Tf_2N]	1.367	1.390	1.646	1.351	1.170	1.389	1.611
[OMI][Tf_2N]	1.292	1.340	3.730	1.298	0.464	1.337	3.476
[PYR][Tf_2N]	1.421	1.443	1.538	1.373	3.378	1.440	1.339

Table 3: Simulation IL density (g/cm^3) comparison to experimental values from publications and literature. An average density is determined for each cutoff parameter. Percent error determined through individual comparison[17-29].

Cutoff (nm)		**0.8**		**1**		**1.2**		**1.4**	
IL	*Exp*	*Sim*	*E (%)*	*Sim*	*E (%)*	*Sim*	*E (%)*	*Sim*	*E (%)*
[BMI][Ac]	1.053	1.028	2.37	1.029	2.27	1.030	2.19	1.030	2.19
[EAM][HCO_2]	1.039	1.099	5.74	1.099	5.78	1.100	5.84	1.099	5.80
[PAM][HCO_2]	0.950	1.049	10.4	1.050	10.5	1.050	10.5	1.051	10.5
[BMI][Tf_2N]	1.436	1.453	1.15	1.455	1.29	1.454	1.27	1.454	1.22
[EMI][Tf_2N]	1.519	1.535	1.02	1.536	1.14	1.537	1.20	1.537	1.18
[HMI][Tf_2N]	1.367	1.387	1.49	1.391	1.73	1.390	1.69	1.390	1.65
[OMI][Tf_2N]	1.292	1.336	3.39	1.338	3.52	1.338	3.54	1.338	3.55
[PYR][Tf_2N]	1.421	1.439	1.29	1.441	1.44	1.441	1.39	1.440	1.33

Figure 3 above shows a plot of overall trends in the data across the full range of simulated parameters of box size and cutoff lengths. Error bars within the plots represent the standard deviation of three simulated replicas. Due to the high reproducibility of the simulations, among different replicas, error bars in figure 3 are too small to be seen behind the point marker. The simulation method estimates the densities of most of the 8 ILs within a few percent with respect to the experimental values. The largest deviation from experimental values occurs for [PAM][HCO_2] (10.5%), followed closely by [EAM][HCO_2] (5.7%) within both the cutoff and box sizing differences. Dnensity tends to be overestimated by these simulations, which is generally the case across simulation methods and force fields reported in literature.

Heat Capacity: Unlike density, the simulations tend to underestimate heat capacities of majority of the ILs. The quantity calculated in this work represents only the excess, or residual (res), portion of the heat capacity, which accounts for the intermolecular interactions in the condensed phase[16]. Conversely, the other portion of the heat capacity is an ideal gas contribution that takes into account intramolecular interactions[16]. The two contributions to the heat capacity are typically calculated as shown in the equation below.

$$< H > = < H^{ig} > + < H^{res} > = < \phi^{int} + K + Nk_{\beta}T > + < \phi^{nb} + PV + Nk_{\beta}T > \quad [3]$$

Typically, ideal gas (ig) portions of heat capacities can be found through experiments, but as this type of experimental data is currently not available for ILs, the values are calculated in literature from a frequency analysis of optimized cation and anion structures from ab initio MD simulations[2, 30]. Since the simulations presented here appear to give fair agreement with experimental heat capacities across a broad range of ILs, the residual heat capacity is the dominating term, and no ideal gas component of the heat capacity is

considered. The data demonstrate that regardless of the parameter changes within the simulation, heat capacity is fairly well estimated as the resulting error was multiplied by 1000. This was done to show there was a level of error presented with each individual IL.

Table 4: Simulation IL heat capacity comparison to experimental values from publications and literature. An average heat capacity is determined for each box size parameter[27, 30-37]. Percent error determined through individual comparison.

Box Size (nm)		**3**		**5**		**10**	
IL	*Exp*	*Sim*	*E (%)*	*Sim*	*E (%)*	*Sim*	*E (%)*
[BMI][Ac]	383	313	18.3	391	2.0	315	17.8
[EAM][HCO_2]	N/A	164	N/A	185	N/A	163	N/A
[PAM][HCO_2]	N/A	191	N/A	289	N/A	345	N/A
[BMI][Tf_2N]	566	391	30.9	532	6.0	417	26.2
[EMI][Tf_2N]	509	349	31.4	456	10.4	345	32.1
[HMI][Tf_2N]	628	454	27.6	591	5.8	469	25.2
[OMI][Tf_2N]	672	510	24.0	663	1.3	523	22.2
[PYR][Tf_2N]	N/A	385	N/A	561	N/A	393	N/A

Table 5: Simulation IL heat capacity comparison to experimental values from publications and literature. An average heat capacity is determined for each box size parameter[27, 30-37]. Percent error determined through individual comparison.

Cutoff (nm)		**0.8**		**1**		**1.2**		**1.4**	
IL	*Exp*	*Sim*	*E (%)*	*Sim*	*E (%)*	*Sim*	*E (%)*	*Sim*	*E (%)*
[BMI][Ac]	383	228	40.4	321	16.2	312	18.5	324	15.5
[EAM][HCO2]	N/A	166	N/A	166	N/A	166	N/A	165	N/A
[PAM][HCO2]	N/A	192	N/A	195	N/A	128	N/A	196	N/A
[BMI][Tf2N]	566	407	28.0	397	29.8	400	29.2	394	30.4
[EMI][Tf2N]	509	353	30.7	351	31.0	346	32.0	347	31.8
[HMI][Tf2N]	628	451	28.1	463	26.3	481	23.3	479	23.6
[OMI][Tf2N]	672	508	24.3	505	24.7	511	23.9	519	22.6
[PYR][Tf2N]	N/A	400	N/A	389	N/A	382	N/A	381	N/A

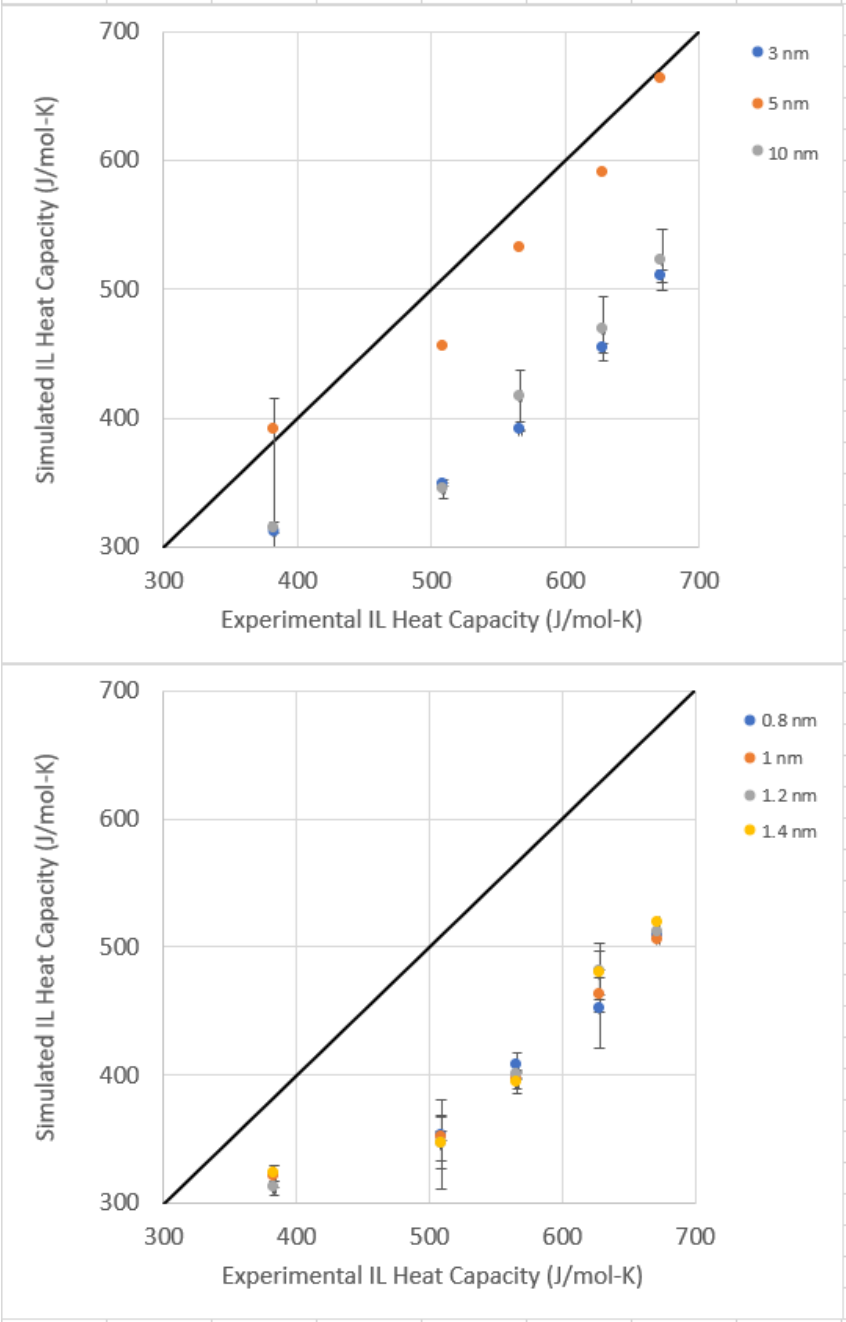

Figure 4: Experimental vs simulated IL heat capacities (J/mol-K). (A) heat capacity for values of box size; (B) heat capacity for values of cutoff.

The heat capacity estimations in this study are less accurate than previous studies upon which the methods were based. Some small differences in the simulations might account for this. For example, in previous work, hydrogen bonds were not constrained, allowing

for their vibrations to contribute to enthalpy fluctuations. Additionally, a different integrator was introduced in GROMACS 5, which might affect the reported enthalpy. Finally, the Berendsen barostat was used in this work, which differs from the more rigorous Parrinello-Rahman barostat used in previous work. The new parameters were selected because they make the simulations more stable and robust. Without constraint of bonds, and with the Parrinello-Rahman barostat, simulations are much more likely to fail with errors. A quick calculation was performed to determine whether these parameters affect the calculated heat capacity, and it was determined that the Berendsen barostat and the constraint of bonds each reduces the enthalpy fluctuations by several percent. These tests were not performed across all ILs and all sets of data, but adherence to older standards might yield more accurate results at the expense of some simulation stability.

Self-Diffusivity: With limited experimental data, the self-diffusivity of only the five [RMIM][Tf_2N] ILs was analyzed. Computed and experimental self-diffusivities for the cation and anion of each of the ILs are reported in Table 6. Fitting for calculation of the self-diffusion coefficients was done over the range 6–10 ns. Figures 6A and 6B present the data graphically; error bars represent the standard deviation of triplicate simulation data. Of all eight ILs only four of had experimental data to be compared with the simulations.

Table 6: Simulation IL self-diffusivity (10^{-11} m^2/sec) comparison to experimental values from publications and literature. An average self-diffusivity is determined for each box size parameter cation and anion. Percent error determined through individual comparison.

Box Size (nm)			**3**			
IL	*cation exp*	*anion exp*	*cation sim*	*Error (%)*	*anion sim*	*Error (%)*
[BMI][Tf2N]	2.76	2.2	4.63	67.9	3.81	73.1
[EMI][Tf2N]	4.98	3.1	7.31	46.8	5.12	65.2
[HMI][Tf2N]	1.69	1.54	3.12	84.5	2.79	81.3
[OMI][Tf2N]	1.17	1.17	3.72	218.3	2.88	145.8
[PYR][Tf2N]	N/A	N/A	6.54	N/A	4.30	N/A

Box Size (nm)			**5**			
IL	*cation exp*	*anion exp*	*cation sim*	*Error (%)*	*anion sim*	*Error (%)*
[BMI][Tf2N]	2.76	2.2	1.13	59.0	0.83	62.2
[EMI][Tf2N]	4.98	3.1	2.29	54.0	1.11	64.1
[HMI][Tf2N]	1.69	1.54	0.87	48.5	0.61	60.3
[OMI][Tf2N]	1.17	1.17	0.41	64.9	0.31	73.5
[PYR][Tf2N]	N/A	N/A	N/A	N/A	N/A	N/A

Box Size (nm)			**10**			
IL	*cation exp*	*anion exp*	*cation sim*	*Error (%)*	*anion sim*	*Error (%)*
[BMI][Tf2N]	2.76	2.2	5.83	111.2	4.55	106.8
[EMI][Tf2N]	4.98	3.1	9.12	83.0	6.60	112.7
[HMI][Tf2N]	1.69	1.54	3.90	130.8	3.38	119.3
[OMI][Tf2N]	1.17	1.17	3.09	163.6	2.84	142.5
[PYR][Tf2N]	N/A	N/A	7.51	N/A	5.53	N/A

Table 7:Simulation IL self-diffusivity (10^{-11} m^2/sec) comparison to experimental values from publications and literature. An average self-diffusivity is determined for each cutoff parameter cation and anion. Percent error determined through individual comparison.

Cutoff (nm)			**0.8**			
IL	*cation exp*	*anion exp*	*cation sim*	*Error (%)*	*anion sim*	*Error (%)*
[BMI][Tf2N]	2.76	2.2	5.31	92.283	4.50	104.500
[EMI][Tf2N]	4.98	3.1	9.41	88.882	9.41	203.430
[HMI][Tf2N]	1.69	1.54	4.12	143.945	4.12	167.706
[OMI][Tf2N]	1.17	1.17	0.38	67.652	3.78	223.476

Cutoff (nm)			**1**			
IL	*cation exp*	*anion exp*	*cation sim*	*Error (%)*	*anion sim*	*Error (%)*
[BMI][Tf2N]	2.76	2.2	5.10	84.626	4.19	90.424
[EMI][Tf2N]	4.98	3.1	9.37	88.246	6.56	111.688
[HMI][Tf2N]	1.69	1.54	3.58	111.815	3.08	99.805
[OMI][Tf2N]	1.17	1.17	3.14	168.034	2.69	129.772

Cutoff (nm)			**1.2**			
IL	*cation exp*	*anion exp*	*cation sim*	*Error (%)*	*anion sim*	*Error (%)*
[BMI][Tf2N]	2.76	2.2	5.74	107.935	4.49	104.030
[EMI][Tf2N]	4.98	3.1	8.16	63.795	5.89	90.108
[HMI][Tf2N]	1.69	1.54	3.44	103.294	3.24	110.325
[OMI][Tf2N]	1.17	1.17	3.42	192.080	2.87	145.356

Cutoff (nm)			**1.4**			
IL	*cation exp*	*anion exp*	*cation sim*	*Error (%)*	*anion sim*	*Error (%)*
[BMI][Tf2N]	2.76	2.2	5.10	84.686	4.25	93.303
[EMI][Tf2N]	4.98	3.1	8.03	61.158	5.44	75.548
[HMI][Tf2N]	1.69	1.54	4.01	137.535	3.41	121.212
[OMI][Tf2N]	1.17	1.17	2.79	138.689	2.58	120.855

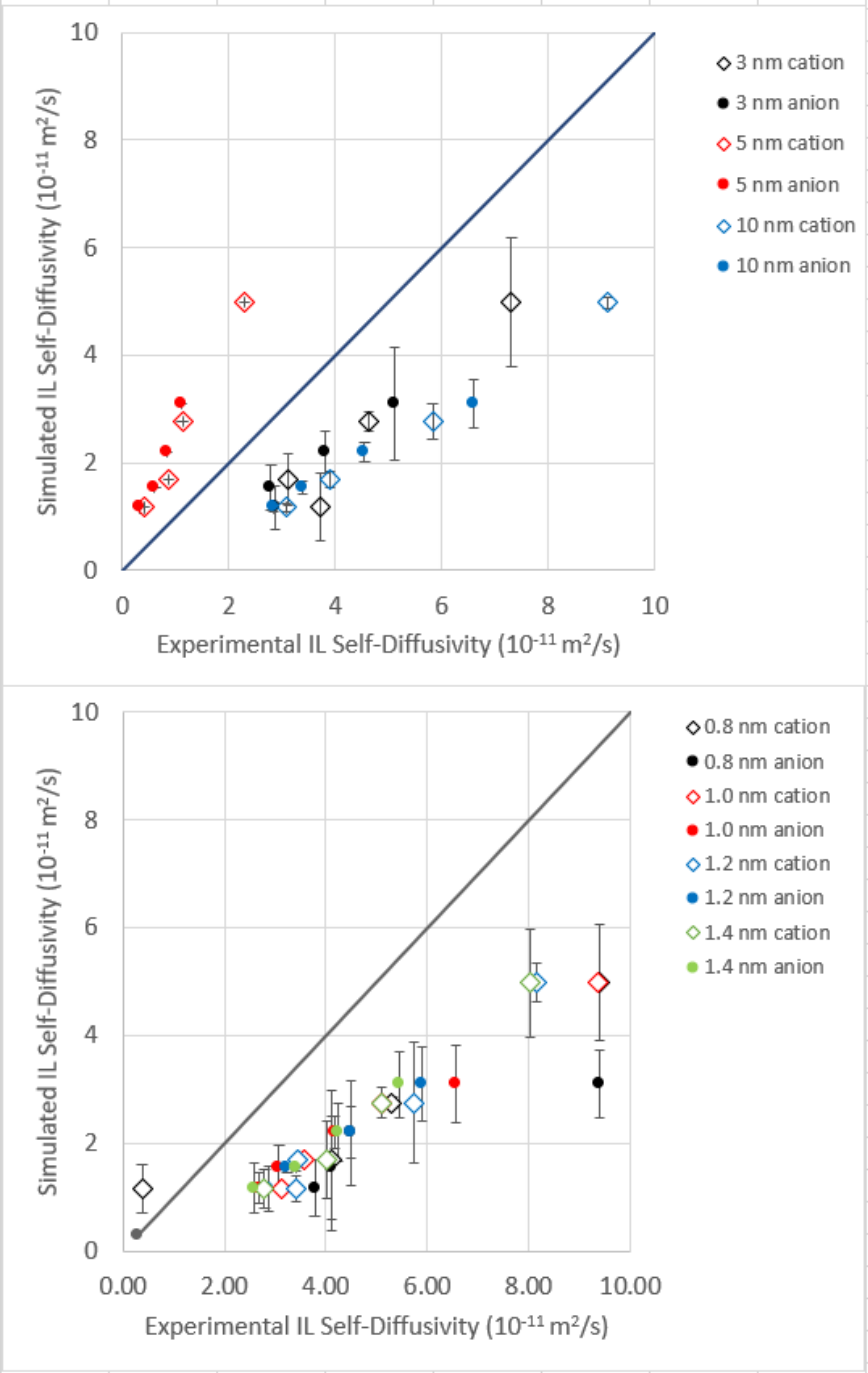

Figure 5: Experimental vs simulated IL self-diffusivities (A) box size (B) cutoff.

The results show that these simulations can accurately determine the trend of decreasing cation/anion self-diffusivity as the cation chain is increasing in length. The trend of decreasing cation/anion self-diffusivity with increasing cation chain length has been observed in other publications. It has been seen that an increased steric hindrance is brought

on by longer cation chain lengths. The simulations are also able to capture an interesting trend of the anion self-diffusivity[16] where self-diffusivity of the [Tf_2N] anion is highest when paired with the fastest cation, [EMIM], while it is the slowest cation, [OMIM], as seen in table 6 and 7. This suggests that cations and anions diffuse through the liquid in pairs or clusters, rather than on their own. For the four IL cation chain lengths tested, the self-diffusivity of the cation at temperature of standard conditions is always higher than that of the anion, though studies show this is not the case for all ILs. Standard deviations in cation/anion self-diffusivity from experiment range from 9 to 73%, shown in table 6 and 7 and graphically in figure 5, meaning that the comparison between simulation and experiment is difficult. Still, because of the notorious difficulty of calculating diffusive properties in ILs, accuracy within a factor of 2-3 is quite good compared to other methods.

In the realm of IL theory, Maginn suggests computing the time-dependent quantity beta, or $\beta(t)$, as a way to measure whether a system is in the diffusive regime[2, 16]. The equation to calculate $\beta(t)$ is shown below.

$$\beta(t) = \frac{dlog(\Delta r^2)}{dlog(t)} \quad [5]$$

The variable t is the simulation time and Δr^2 is the MSD of the ion centers of mass, as in equation 4. The system can be said to have reached diffusive behavior when $\beta(t)$ has reached a value of 1; values below 1 indicate sub diffusive behavior. The simulations of [RMIM][Tf_2N] (R = E, B, and H) all reached diffusive behavior after 5 ns. Simulations of [OMIM][Tf_2N], however, never reached diffusive behavior over the 10 ns; Thus, for ILs with long-chained ions, such as [OMIM][Tf_2N], the simulation can be extended farther then the initial set point to have better results through extended simulation time, or

increased simulation temperature, to have more confidence in the calculated ion self-diffusivities. Of the four [RMIM] cations, the greatest percent error relative to experiment is seen for [OMIM].

IV. EFFICENCY ANALYSIS

To determine the speed of the calculations, the md.log file was accessed. The simulation speed is measured in ns per day. Simulations in this study were run on the high-performance computing environment at the University of Louisville, which contains over 500 compute nodes. The nodes used in this study contained a pair of Intel E5420 processors at 2.50 GHz. Because these chips are several years old, the computational power of this pair of chips is equivalent to a modern midrange desktop computer, similar to those used by faculty and staff.

One of the ILs was selected at random for the efficiency analysis. Times of each simulation were extracted for box size and cutoff. The results demonstrate that the smaller the box is the faster the simulation will run. Similarly, a smaller cutoff corresponds to a higher speed. This makes sense, since the smaller box sizes require the integration of the equations of motion for fewer molecules, and smaller cutoffs mean fewer intermolecular interactions need to be calculated. Simulation throughput is presented in Table 8. The module was run and its output compared to the previously collected data.

Table 8: Simulation efficiency for [EAM][HCO_2]. Parameters used in previous simulations are indicated in bold italics.

[EAM][HCO_2]	*Box Size (nm)*	*Cutoff (ns)*	*time (ns/day)*
	3	1.2	128.1
	5	***1.2***	***69.1***
	10	1.2	4.1

[EAM][HCO_2]	*Box Size (nm)*	*Cutoff (ns)*	*time (ns/day)*
	5	0.8	118.4
	5	1	91.8
	5	***1.2***	***69.1***
	5	1.4	51.5

To determine the increase in simulation efficiency the throughput was first compared for box size where there was an increase in efficiency of a factor of 1.9, meaning the simulations ran 1.9 faster with a box size of size-length 3 nm compared to 5 nm. Even with a smaller box size, the thermophysical properties predicted by these simulations do not change significantly. Therefore, it is suggested that a box size of 3 nm is sufficient to capture these properties. Changing the cutoff range from 1.2 nm to 0.8 nm yields an improvement factor of 1.7. Once again, there is no significant change in the calculated properties across the range of cutoff values. Therefore it is also suggested that the box cutoff be reduced to 0.8 nm. Taken together, these improvements mean that a simulation

can be run 3.2 times faster than previously reported studies without greatly sacrificing simulation accuracy.

V. CONCLUSIONS

The properties of density, heat capacity, and self-diffusivity of eight ionic liquids have been calculated using molecular dynamics with the general AMBER force field. Results have been compared to experimental values. Simulations predicted higher density and lower heat capacity than experimental work, with typical deviations of a few to several percent for density and 20-30 percent for heat capacity. There was however a greater error in the calculated IL transport properties of cation and anion self-diffusivity. Transport properties are notoriously difficult to calculate from simulations, and such a deviation is to be expected. Qualitative trends of decreasing self-diffusivity with a longer cation chain length were observed in agreement with experiment and previously published simulations. Taken altogether, with respect to previously published work, in this study thermodynamic and transport properties of ILs are predicted quite accurately even with changes to very important simulation parameters.

This work demonstrates that the accuracy of simulated values does not drop with moderately less stringent simulation parameters (i.e. smaller box size and shorter non-bonded cutoffs) than previously published work. Smaller box sizes and shorter cutoff lengths, if paired appropriately, can achieve an increase in simulation efficiency by a factor of approximately 3.2. This study demonstrates that several important properties of a given

IL species can be predicted easily on a standard desktop computer within a matter of hours, providing a pathway to speed the discovery of novel solvents.

VI. REFERENCES

1. Holbrey, J. D.; Reichert, W. M.; Rogers, R. D., Crystal structures of imidazolium bis(trifluoromethanesulfonyl)imide 'ionic liquid' salts: the first organic salt with a cis-TFSI anion conformation. *Dalton Transactions* **2004,** (15), 2267-2271.

2. Sprenger, K. G.; Jaeger, V. W.; Pfaendtner, J., The General AMBER Force Field (GAFF) Can Accurately Predict Thermodynamic and Transport Properties of Many Ionic Liquids. *The Journal of Physical Chemistry B* **2015,** *119* (18), 5882-5895.

3. Mattedi, S.; Carvalho, P. J.; Coutinho, J. A. P.; Alvarez, V. H.; Iglesias, M., High pressure CO2 solubility in N-methyl-2-hydroxyethylammonium protic ionic liquids. *The Journal of Supercritical Fluids* **2011,** *56* (3), 224-230.

4. Plechkova, N. V.; Seddon, K. R., Applications of ionic liquids in the chemical industry. *Chemical Society Reviews* **2008,** *37* (1), 123-150.

5. Wilkes, J. S., A short history of ionic liquids-from molten salts to neoteric solvents. *Green Chemistry* **2002,** *4* (2), 73-80.

6. Liu, Z. C.; Meng, X. H.; Zhang, R.; Xu, C. M., Friedel-Crafts Acylation of Aromatic Compounds in Ionic Liquids. *Petroleum Science and Technology* **2009,** *27* (2), 226-237.

7. Ionic Liquids. In *Kirk-Othmer Encyclopedia of Chemical Technology*.

8. Páll, S.; Abraham, M. J.; Kutzner, C.; Hess, B.; Lindahl, E. In *Tackling Exascale Software Challenges in Molecular Dynamics Simulations with GROMACS*, Solving Software Challenges for Exascale, Cham, 2015//; Markidis, S.; Laure, E., Eds. Springer International Publishing: Cham, 2015; pp 3-27.

9. Friederich, P.; Konrad, M.; Strunk, T.; Wenzel, W., Machine learning of correlated dihedral potentials for atomistic molecular force fields. *Scientific Reports* **2018,** *8* (1), 2559.

10. Li, Y.; Li, H.; Pickard, F. C.; Narayanan, B.; Sen, F. G.; Chan, M. K. Y.; Sankaranarayanan, S. K. R. S.; Brooks, B. R.; Roux, B., Machine Learning Force Field Parameters from Ab Initio Data. *Journal of Chemical Theory and Computation* **2017,** *13* (9), 4492-4503.

11. González, M. A., Force fields and molecular dynamics simulations. *JDN* **2011,** *12*, 169-200.

12. Zhang, Y.; Maginn, E. J., A Simple AIMD Approach to Derive Atomic Charges for Condensed Phase Simulation of Ionic Liquids. *The Journal of Physical Chemistry B* **2012,** *116* (33), 10036-10048.

13. Youngs, T. G.; Hardacre, C., Application of static charge transfer within an ionic-liquid force field and its effect on structure and dynamics. *Chemphyschem : a European journal of chemical physics and physical chemistry* **2008,** *9* (11), 1548-58.

14. Yoo Willow, S.; A Salim, M.; Kim, K.; Hirata, S., *Ab initio molecular dynamics of liquid water using embedded-fragment second-order many-body perturbation theory towards its accurate property prediction*. 2015; Vol. 5, p 14358.

15. Wang, J.; Wang, W.; Kollman, P. A.; Case, D. A., Automatic atom type and bond type perception in molecular mechanical calculations. *Journal of Molecular Graphics and Modelling* **2006,** *25* (2), 247-260.

16. Maginn, E. J., Atomistic Simulation of the Thermodynamic and Transport Properties of Ionic Liquids. *Accounts of Chemical Research* **2007,** *40* (11), 1200-1207.

17. Araújo, J. M. M.; Pereiro, A. B.; Alves, F.; Marrucho, I. M.; Rebelo, L. P. N., Nucleic acid bases in 1-alkyl-3-methylimidazolium acetate ionic liquids: A thermophysical and ionic conductivity analysis. *The Journal of Chemical Thermodynamics* **2013,** *57*, 1-8.

18. Dzida, M.; Chorążewski, M.; Geppert-Rybczyńska, M.; Zorębski, E.; Zorębski, M.; Żarska, M.; Czech, B., Speed of Sound and Adiabatic Compressibility of 1-Ethyl-3-methylimidazolium Bis(trifluoromethylsulfonyl)imide under Pressures up to 100 MPa. *Journal of Chemical & Engineering Data* **2013,** *58* (6), 1571-1576.

19. Fröba, A. P.; Rausch, M. H.; Krzeminski, K.; Assenbaum, D.; Wasserscheid, P.; Leipertz, A., Thermal Conductivity of Ionic Liquids: Measurement and Prediction. *International Journal of Thermophysics* **2010,** *31* (11), 2059-2077.

20. Greaves, T. L.; Weerawardena, A.; Fong, C.; Krodkiewska, I.; Drummond, C. J., Protic Ionic Liquids: Solvents with Tunable Phase Behavior and Physicochemical Properties. *The Journal of Physical Chemistry B* **2006,** *110* (45), 22479-22487.

21. Harris, K. R.; Kanakubo, M.; Woolf, L. A., Temperature and Pressure Dependence of the Viscosity of the Ionic Liquids 1-Hexyl-3-methylimidazolium Hexafluorophosphate and 1-Butyl-3-methylimidazolium Bis(trifluoromethylsulfonyl)imide. *Journal of Chemical & Engineering Data* **2007,** *52* (3), 1080-1085.

22. Kato, R.; Gmehling, J., Systems with ionic liquids: Measurement of VLE and $\gamma\infty$ data and prediction of their thermodynamic behavior using original UNIFAC, mod. UNIFAC(Do) and COSMO-RS(Ol). *The Journal of Chemical Thermodynamics* **2005,** *37* (6), 603-619.

23. Krummen, M.; Wasserscheid, P.; Gmehling, J., Measurement of Activity Coefficients at Infinite Dilution in Ionic Liquids Using the Dilutor Technique. *Journal of Chemical & Engineering Data* **2002,** *47* (6), 1411-1417.

24. Nieto de Castro, C.; Langa, E.; Morais, A.; Lopes, M.; Lourenco, M.; Santos, F.; Santos, M.; Canongia Lopes, J. N.; I. M. Veiga, H.; Macatrão, M.; Esperança, J.; Marques, C.; Rebelo, L.; A. M. Afonso, C., *Studies on the density, heat capacity, surface tension and infinite dilution diffusion with the ionic liquids [C(4)mim][NTf(2)], [C(4)mim][dca], [C(2)mim][EtOSO(3)] and [Aliquat][dca]*. 2010; Vol. 294, p 157-179.

25. Seki, S.; Tsuzuki, S.; Hayamizu, K.; Umebayashi, Y.; Serizawa, N.; Takei, K.; Miyashiro, H., Comprehensive Refractive Index Property for Room-Temperature Ionic Liquids. *Journal of Chemical & Engineering Data* **2012,** *57* (8), 2211-2216.

26. Shiflett, M. B.; Harmer, M. A.; Junk, C. P.; Yokozeki, A., Solubility and Diffusivity of Difluoromethane in Room-Temperature Ionic Liquids. *Journal of Chemical & Engineering Data* **2006,** *51* (2), 483-495.

27. Troncoso, J.; Cerdeiriña, C. A.; Sanmamed, Y. A.; Romaní, L.; Rebelo, L. P. N., Thermodynamic Properties of Imidazolium-Based Ionic Liquids: Densities, Heat Capacities, and Enthalpies of Fusion of [bmim][PF6] and [bmim][NTf2]. *Journal of Chemical & Engineering Data* **2006,** *51* (5), 1856-1859.

28. Vranes, M.; Dozic, S.; Djeric, V.; Gadzuric, S., Physicochemical Characterization of 1-Butyl-3-methylimidazolium and 1-Butyl-1-methylpyrrolidinium Bis(trifluoromethylsulfonyl)imide. *Journal of Chemical & Engineering Data* **2012,** *57* (4), 1072-1077.

29. Widegren, J. A.; Magee, J. W., Density, Viscosity, Speed of Sound, and Electrolytic Conductivity for the Ionic Liquid 1-Hexyl-3-methylimidazolium Bis(trifluoromethylsulfonyl)imide and Its Mixtures with Water. *Journal of Chemical & Engineering Data* **2007,** *52* (6), 2331-2338.

30. Cadena, C.; Zhao, Q.; Snurr, R. Q.; Maginn, E. J., Molecular Modeling and Experimental Studies of the Thermodynamic and Transport Properties of Pyridinium-Based Ionic Liquids. *The Journal of Physical Chemistry B* **2006,** *110* (6), 2821-2832.

31. Crosthwaite, J. M.; Muldoon, M. J.; Dixon, J. K.; Anderson, J. L.; Brennecke, J. F., Phase transition and decomposition temperatures, heat capacities and viscosities of pyridinium ionic liquids. *The Journal of Chemical Thermodynamics* **2005,** *37* (6), 559-568.

32. García-Miaja, G.; Troncoso, J.; Romaní, L., Excess properties for binary systems ionic liquid+ethanol: Experimental results and theoretical description using the ERAS model. *Fluid Phase Equilibria* **2008,** *274* (1), 59-67.

33. Ge, R.; Hardacre, C.; Jacquemin, J.; Nancarrow, P.; Rooney, D. W., Heat Capacities of Ionic Liquids as a Function of Temperature at 0.1 MPa. Measurement and Prediction. *Journal of Chemical & Engineering Data* **2008,** *53* (9), 2148-2153.

34. Rocha, M. A. A.; Bastos, M.; Coutinho, J. A. P.; Santos, L. M. N. B. F., Heat capacities at 298.15K of the extended [CnC1im][Ntf2] ionic liquid series. *The Journal of Chemical Thermodynamics* **2012,** *53*, 140-143.

35. Shimizu, Y.; Ohte, Y.; Yamamura, Y.; Saito, K.; Atake, T., Low-Temperature Heat Capacity of Room-Temperature Ionic Liquid, 1-Hexyl-3-methylimidazolium

Bis(trifluoromethylsulfonyl)imide. *The Journal of Physical Chemistry B* **2006,** *110* (28), 13970-13975.

36. Strechan, A. A.; Paulechka, Y. U.; Blokhin, A. V.; Kabo, G. J., Low-temperature heat capacity of hydrophilic ionic liquids [BMIM][CF3COO] and [BMIM][CH3COO] and a correlation scheme for estimation of heat capacity of ionic liquids. *The Journal of Chemical Thermodynamics* **2008,** *40* (4), 632-639.

37. Yoshitaka, S.; Yoko, O.; Yasuhisa, Y.; Kazuya, S., Effects of Thermal History on Thermal Anomaly in Solid of Ionic Liquid Compound, [C4mim][Tf2N]. *Chemistry Letters* **2007,** *36* (12), 1484-1485.

APPENDIX